The Effect of Local Sea Surface Temperatures on Atmospheric Circulation over the Tropical Atlantic Sector

PING CHANG

Department of Oceanography, Texas A&M University, College Station, Texas

R. SARAVANAN

National Center for Atmospheric Research, Boulder, Colorado

LINK JI

Department of Oceanography, Texas A&M University, College Station, Texas

G. C. HEGERL

JISAO, University of Washington, Seattle, Washington

(Manuscript received 17 February 1999, in final form 8 August 1999)

ABSTRACT

The effects of tropical Atlantic sea surface temperature (SST) anomalies on atmospheric circulation are examined by analyzing several ensembles of integrations of an atmospheric general circulation model (AGCM) forced with differently configured SSTs. An attempt is made to separate the atmospheric response to local SST forcing from internal atmospheric variability, using various statistical analyses. The analyses reveal a robust pattern of atmospheric response to SST forcing. The dominant response is largely confined within the tropical Atlantic sector and may be associated with the variation in location and intensity of the intertropical convergence zone (ITCZ) in response to changes in SST gradient near the equator. Within the deep Tropics, particularly in the western tropical Atlantic warm pool region, there is an indication of a positive feedback between surface heat flux and SST anomalies. In this warm SST region, the latent heat flux tends to dominate surface heat flux variability, and the positive feedback takes place between the wind-induced flux and SST. Outside the deep Tropics, surface heat flux generally tends to dampen the SST, indicating a negative feedback. A strong negative feedback is found off the coast of west Saharan Africa, where the mean SST is cold and the surface heat flux variability is largely induced by the air–sea temperature difference. The forced response exhibits a seasonal dependence. The structure throughout the year bears a close resemblance to the winter pattern, suggesting that the anomalies during the boreal winter contribute to much of the year-to-year variability in the tropical Atlantic sector. An ENSO-like response in the tropical Atlantic is also identified. It appears as the second dominant forced response and has its strongest manifestation during the boreal fall. By comparing the responses of different sets of ensemble experiments, it is found that the dominant near-surface atmospheric response in the tropical Atlantic sector primarily comes from the local SST forcing. A significant remote influence of the Pacific ENSO on the tropical Atlantic variability is also noted. The strongest remote influence from the tropical Pacific occurs during the boreal spring. The companion paper by Saravanan and Chang further explores the effect of ENSO using an index-based regression analysis.

1. Introduction

It is widely recognized that the SST anomalies in the tropical Pacific have a dramatic impact on atmospheric circulation. Extensive studies have been performed to understand atmospheric responses to El Niño–related SST anomalies in the tropical Pacific (see Trenberth et al. 1998 for a recent review). In contrast, the direct impact of SST anomalies in the tropical Atlantic Ocean on atmospheric circulation is less well studied despite the fact that there is extensive literature that points to a close link between climate variability in countries surrounding the tropical Atlantic basin and local SST anomalies [see Hastenrath (1985) for an overview]. For example, the well-known droughts of northeast Brazil have been shown to be closely related to variability of the cross-equatorial SST gradient (Hastenrath and Heller

Corresponding author address: Dr. Ping Chang, Department of Oceanography, Texas A&M University, College Station, Texas 77843-3160.
E-mail: ping@ocean.tamu.edu

1977; Moura and Shukla 1981; Hastenrath 1985; Lough 1986; Rao et al. 1993; Harzallah et al. 1996; Mehta 1998). The interhemispheric SST anomalies are also found to have an effect on rainfall variability in sub–Saharan Africa (Lamb 1978a,b; Hastenrath and Lamb 1977; Folland et al. 1986) and Central American–Caribbean regions (Hastenrath 1976; Enfield 1996; Giannini et al. 1998; Saravanan and Chang 2000).

The finding that the regional climate variability and the tropical Atlantic SSTs are significantly correlated implies that the latter exert a considerable influence on the atmospheric circulation. However, because tropical Atlantic variability may also be remotely forced by El Niño–Southern Oscillation (ENSO) in the tropical Pacific and North Atlantic oscillation (NAO) in the high-latitude Atlantic, how much direct influence the tropical Atlantic SSTs have on the atmosphere is not entirely clear. An earlier atmospheric general circulation model (AGCM) study by Moura and Shukla (1981) shows that the location and intensity of the intertropical convergence zone (ITCZ) are affected by the tropical Atlantic SST anomalies, which in turn influence northeast Brazilian rainfall variability. Modeling evidence on the importance of the SST anomalies in Sahel rainfall has also been presented (Folland et al. 1986). A more recent AGCM study by Robertson et al. (1998) further suggests that the effect of tropical Atlantic SSTs may reach beyond the tropical region, and the NAO may be remotely influenced by tropical Atlantic SST variability.

In spite of these previous efforts, currently there is a lack of a systematic examination of the importance of tropical Atlantic SST influence on the atmospheric circulation. One of the objectives of the present study is to address this issue. We will analyze the responses of three ensembles of integrations of the Community Climate Model (CCM3) developed at the National Center for Atmospheric Research (NCAR) in an attempt to determine the atmospheric response to local SST forcing in the tropical Atlantic. Each set of experiments differs in the geographic distribution of the SST forcing. In the first set of experiments, SST forcing is specified throughout the global oceans. In the second set of experiments, SST forcing is specified within the global tropical oceans. Finally, in the third experiment, SST forcing is specified only in the tropical Atlantic Ocean. A comparison of these experiments allows us to determine the relative importance between local SST influence from the tropical Atlantic and remote SST influence from the other oceans. The focus of this paper is on the effect of local SSTs on the atmospheric circulation in the tropical Atlantic sector. The remote effects, particularly those associated with the Pacific ENSO, are the main subject of the companion paper by Saravanan and Chang (2000).

The other objective of this study is to gain understanding of various air–sea feedbacks in the tropical Atlantic region. Air–sea feedbacks have been hypothesized to be an important contributing factor to tropical Atlantic variability. A positive feedback means that the atmosphere and oceans are mutually reinforcing each other and thereby the two media are coupled. A negative feedback usually indicates that the atmosphere is merely forcing the oceans. In this study, we attempt to determine the regions where the different types of feedback take place in the tropical Atlantic and to explore the physical mechanisms that are responsible for these feedbacks.

One of the feedback mechanisms that may be of particular interest to tropical Atlantic variability is the positive feedback between the meridional SST gradient near the equator and the latent heat flux anomaly induced by changes in trade wind strength (Chang et al. 1997; Carton et al. 1996). At the present, the importance of this positive feedback process in tropical Atlantic climate variability remains controversial. Relatively simple coupled model studies (Chang et al. 1997; Xie and Tanimoto 1998) suggest that the positive feedback may be fundamental for the decadal variation in the tropical Atlantic. These simple models, however, do not include complete physics of the real system. The importance of air–sea feedback could be exaggerated in these models. The current fully coupled GCMs, on the other hand, provide little evidence for a coupled decadal oscillation in the tropical Atlantic. This leads to the possibility that the tropical Atlantic variability may be largely forced by the internal atmospheric variability (Dommenget and Latif 2000; Delworth and Mehta 1998). Although the coupled GCMs include more complete physics, they are imperfect; without a flux adjustment, the mean states of these models, particularly in the eastern equatorial Pacific and Atlantic, present a severe problem (Mechoso et al. 1995), which could distort the coupled physics.

The basic requirements for a positive air–sea feedback are 1) the atmosphere must respond to SST anomalies and 2) the induced anomalous atmospheric circulation must produce a net forcing to enhance the SST anomalies. These requirements can be examined systematically in a stand-alone AGCM forced with specified SSTs, provided that the forced atmospheric response can be separated from internal atmospheric variability. Identifying a reliable forced atmospheric response to SST forcing is not a trivial matter, particularly in the extratropics, where internal atmospheric variability is strong (Palmer and Sun 1985; Kushnir and Held 1996; Peng et al. 1997; Saravanan 1998). The weak forced signal and strong internal variability present a signal-to-noise problem (Davies et al. 1997). To overcome this problem, Venzke et al. (1999) employed a signal-to-noise maximizing EOF analysis (Allen and Smith 1997) to an ensemble of multidecadal AGCM integrations and successfully extracted a forced atmospheric response in the North Atlantic sector. The signal-to-noise maximizing EOF analysis is related to optimal detection techniques used to detect forced signals in observations (Hasselmann 1979) and to prewhitening techniques used in general signal-processing approaches, where the noise is

prewhitened to detect a covarying signal. In this study, we will apply this optimal detection algorithm to dissect coupled mechanisms in the tropical Atlantic sector.

In the companion paper (Saravanan and Chang 2000), where the focus is on the remote influence of ENSO, we use a traditional index-based regression analysis. This simple method is effective for identifying the remote effects of ENSO because ENSO is the predominant climate mode of variability in the tropical Pacific and can be characterized by simple indexes such as the Niño-3 SST index. In contrast to ENSO, tropical Atlantic variability behaves in a more complex manner and may involve local feedbacks and interactions with other climatic modes such as ENSO and the NAO. The local feedback signal in the tropical Atlantic is expected to be weaker than the Pacific counterpart, making it generally more difficult to characterize tropical Atlantic variability using a simple index. Consequently, an index-based regression analysis is less effective in analyzing local air–sea interaction in the tropical Atlantic. A data adoptive technique is highly desirable to assure the robustness of the findings of the simple analysis. The signal-to-noise maximizing EOF analysis is ideally suited for separating a local air–sea feedback signal from the internal atmospheric variability. As will be shown, the results obtained in this study are complementary to those of the companion paper (Saravanan and Chang 2000), despite the fact that they are obtained via very different analysis techniques. This points to the robustness of the conclusions.

The arrangement of the paper is as follows: section 2 describes the model and experiment setup, section 3 compares simulated annual mean states with observations in the tropical Atlantic sector, section 4 discusses the simulated precipitation in comparison to the observation, section 5 explains how to extract the dominant forced response from an ensemble of integrations and presents the results from the tropical Atlantic Ocean, and section 6 summarizes and discusses the major findings. An appendix outlines the analysis method and implementation.

2. Model and experiments

Several ensembles of CCM3 integrations were performed at NCAR. CCM3 is a state-of-the-art AGCM incorporating a comprehensive suite of physical parameterizations, including a nonlocal boundary layer parameterization and improved radiative and convective parameterizations (Kiehl et al. 1998). Land surface processes in CCM3 are represented by a fully interactive land model (Bonan 1998). The mean atmospheric flow as simulated by uncoupled integrations of CCM3, including the zonal-mean temperature and velocity fields and the stationary wave structure, compares favorably with observations and has a fairly small amount of systematic errors (Hurrell et al. 1998). CCM3 also provides a fairly good simulation of atmospheric low-frequency variability (Saravanan 1998). The standard configuration of CCM3 used in this study has T42 spectral truncation in the horizontal and 18 levels in the vertical.

The difference among various sets of integrations is in the specification of SST forcing. The results presented in this study are based on three ensembles of CCM3 runs forced with differently configured observed SSTs and an additional run forced with climatological SSTs. The following is a brief description of each experiment. An acronym is coined for each set of experiments for brevity.

- Annual Cycle of SST (ACYC) experiment: This experiment consists of a single 145-yr CCM3 run forced with climatological SSTs in the global oceans. Since SST anomalies are absent in this experiment, the atmospheric variability is generated completely by internal dynamics. Thus, the output of this experiment provides an estimate of internal atmospheric variability in CCM3.
- Global Ocean Global Atmosphere (GOGA) experiment: This set of experiments consists of an ensemble of 10 CCM3 integrations forced with monthly averaged observed SSTs (Smith et al. 1996) in the global oceans from January 1950 to December 1994. Each integration started from a different initial condition of the atmosphere.
- Tropical Ocean Global Atmosphere (TOGA) experiment: This set of experiments consists of an ensemble of five CCM3 integrations forced with the same SSTs as in GOGA except only in the global tropical oceans between 30°S and 30°N. Outside the tropics, the SSTs were gradually damped (by a simple linear extrapolation) to climatological SSTs between 30° and 40° in both hemispheres. Beyond 40°S and 40°N, climatological SST values were assigned.
- Tropical Atlantic Ocean Global Atmosphere (TAGA) experiment: This set of experiments consists of an ensemble of five CCM3 integrations forced with the same SSTs except that the forcing is specified only in the tropical Atlantic Ocean between 18°S and 18°N. Similar to the TOGA experiment, there is a 10°-wide transition zone in each hemisphere where SSTs were gradually damped to the climatological values. Climatological SST values were assigned elsewhere in the global oceans.

Because our main interests are in the tropical Atlantic Ocean, all the analyses presented below are in a domain from 30°S to 45°N and from 80°W to 20°E. The simulated datasets have been converted into monthly averages and interpolated onto a $2° \times 2°$ grid.

3. Simulated mean circulations

Much of the tropical Atlantic variability is closely associated with the variation of the location and intensity of the ITCZ. It is thus important that the AGCM is capable of simulating the mean circulation and the

ITCZ in the tropical Atlantic basin. For this reason, we first examined the simulated annual mean fields and compared the results with the Comprehensive Ocean Atmosphere Data Sets (COADS) compiled by da Silva et al. (1994) and the National Center for Environmental Prediction (NCEP)–NCAR 40-Year Reanalysis datasets (Kalnay et al. 1996).

All the annual mean fields except precipitation were computed based on monthly mean data from January 1960 to December 1989. The simulated annual mean fields were also based on ensemble averages. In the following discussion, only the mean circulations from the GOGA experiment are displayed because the annual mean fields in the other two sets of experiments are virtually identical to those of GOGA experiment.

Figure 1 shows the simulated and observed annual mean fields of the zonal and meridional components of the wind stress, τ^x and τ^y, as well as the net surface heat flux. It is evident that the CCM3 simulation realistically reproduces the patterns of the annual mean fields, especially the zonal component τ^x. However, the strength of the wind stresses is generally overestimated by the model, particularly outside the Tropics. For example, the simulated meridional wind stress τ^y between 30° and 45°N is three times stronger than the observed values. A close inspection of τ^y indicates that the tropical convergence zone (approximated by the zero contour lines of τ^y near the equator) exhibits a slightly more southwest-to-northeast tilt in the simulations than in reality. Overall, the surface circulation over the tropical Atlantic Ocean is well represented by the model.

The overall spatial pattern of the simulated heat flux also agrees very well with COADS and the NCEP–NCAR 40-Year Reanalysis. Positive heat fluxes are found within the equatorial zone and along the eastern boundaries while large negative fluxes are found along the Gulf Stream. In comparison with COADS, the values of simulated net surface heat flux appear to be smaller than the observed values by about 20 W m^{-2}, which may be attributed to the overestimation of surface wind speed, leading to an overestimation of evaporation in the model. The area where the largest discrepancy between the observed and simulated annual mean fluxes occurs is in the northern tropical Atlantic, where COADS indicates near-zero values of net surface heat flux while the CCM3 simulations show a negative flux value of 20 W m^{-2}. Interestingly, NCEP–NCAR 40-Year Reanalysis gives an even larger negative heat flux value in that region. Given large uncertainties in surface heat flux estimates (da Silva et al. 1994) it is gratifying that the heat flux simulated by the CCM3 is at least consistent with those in COADS and NCEP–NCAR 40-Year Reanalysis.

4. Simulated precipitation

Precipitation is a good measure of the location and intensity of the ITCZ and thus serves as a useful gauge for the model's performance in simulating tropical convection and circulation. The simulated precipitation from the GOGA experiment is compared with the observed global precipitation data compiled by Xie and Arkin (1996). Since the period of the observed precipitation (January 1979–December 1995) overlaps with that of the simulation from January 1979 to December 1994, 16-yr monthly averaged precipitation data from that period were used in the comparison. Figure 2 shows the annual mean precipitation. It is evident that the model correctly captures both the intensity and location of the ITCZ in the tropical Atlantic region. The simulated precipitation appears to be somewhat stronger than the observed values over the continents; however, it is weaker in the ocean's interior. Compared to the observation, the heavy precipitation band over the ocean is shifted too far westward and spread too far southward along the Brazilian coast. In spite of these shortcomings, the CCM3 successfully reproduces major features of the ITCZ over the Atlantic sector.

Figure 3 depicts the annual cycle of precipitation. The seasonal variation of the precipitation associated with the north–south migration of the ITCZ is well captured by the model. Overall, the annual cycle of precipitation over the ocean is better simulated than that over land, and the precipitation during boreal winter and spring is better simulated than that during summer and fall. Some of the major deficiencies of the model are that the wintertime increase of precipitation over eastern-central Brazil is overestimated by the model, the summer rainfall over west Africa is underestimated, and the precipitation over central America and the Caribbean is overestimated.

The variability of the simulated and observed precipitation anomalies are compared in terms of leading EOFs (not shown). The overall spatial patterns of the leading EOFs show a good agreement between the observation and simulation over the ocean. However, the agreement over the land is less satisfactory. In both simulation and observation, the leading EOFs show a predominantly dipolelike structure over the tropical Atlantic Ocean, suggesting that the precipitation anomalies are mainly associated with the north–south movement of the ITCZ. The principal components of the EOFs are highly correlated with the cross-equatorial gradient of the anomalous SST in the region (not shown). In fact, one can obtain a similar precipitation pattern by regressing the precipitation anomalies onto a tropical Atlantic SST index, as shown in Saravanan and Chang (2000). It will be shown in the following section that this precipitation pattern is indeed a response to the local SST forcing in the tropical Atlantic. The second EOFs show a more symmetric pattern about the equator (not shown). Much of the precipitation variability contained in the second EOFs is associated with ENSO-related SST variability in the tropical Pacific. The spatial structure of the second EOFs bears a close resemblance to the regression of precipitation anomalies onto the Niño-3 SST index

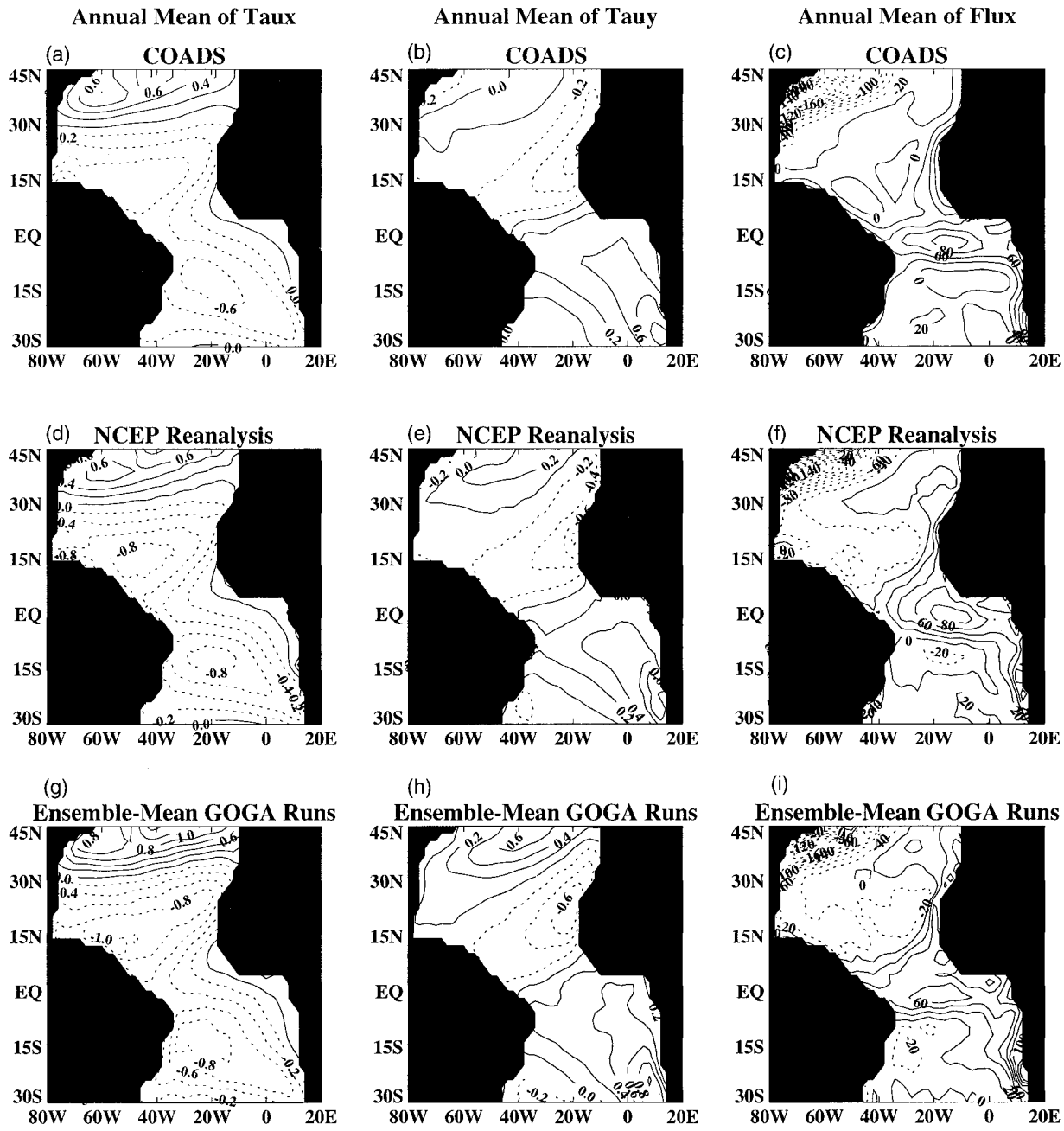

FIG. 1. Comparison of annual mean wind stresses and net surface heat flux among COADS (upper panels), NCEP–NCAR 40-Year Reanalysis (middle panels), and the ensemble mean of CCM3 GOGA runs (bottom panels). The contour intervals for the zonal and meridional wind stresses (left and middle panels) are 0.2 dyn cm^{-2}. The contour interval for the heat fluxes (right panels) is 20 W m^{-2}.

shown in the companion paper (Saravanan and Chang 2000).

In summary, we conclude that the annual mean and seasonal cycle as well as interannual variability of the precipitation over the tropical Atlantic sector are reasonably well simulated by the model. In the next section, we will further analyze anomalous circulation to isolate the atmospheric response to local SST forcing.

5. Dominant forced response

The atmospheric variability can be divided into two parts: an internal part that is governed by internal dynamics of the atmosphere and is independent of anomalous SST forcing, and an external part that is driven by SST anomalies. The internal part can be considered as the ''noise'' for the present problem because this part

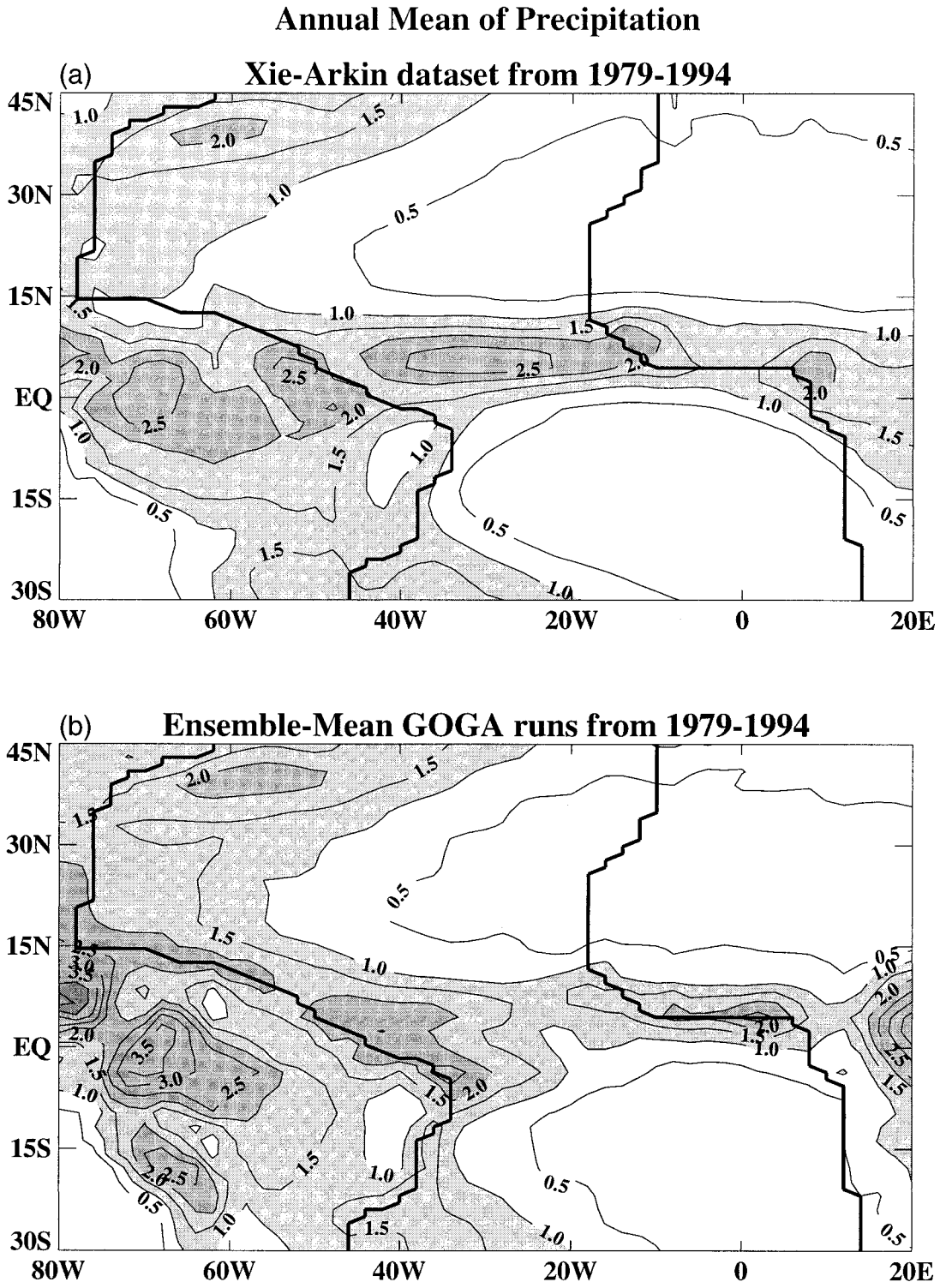

FIG. 2. Observed and simulated annual mean precipitation in the tropical Atlantic sector. The contour interval is 0.5 m yr^{-1}.

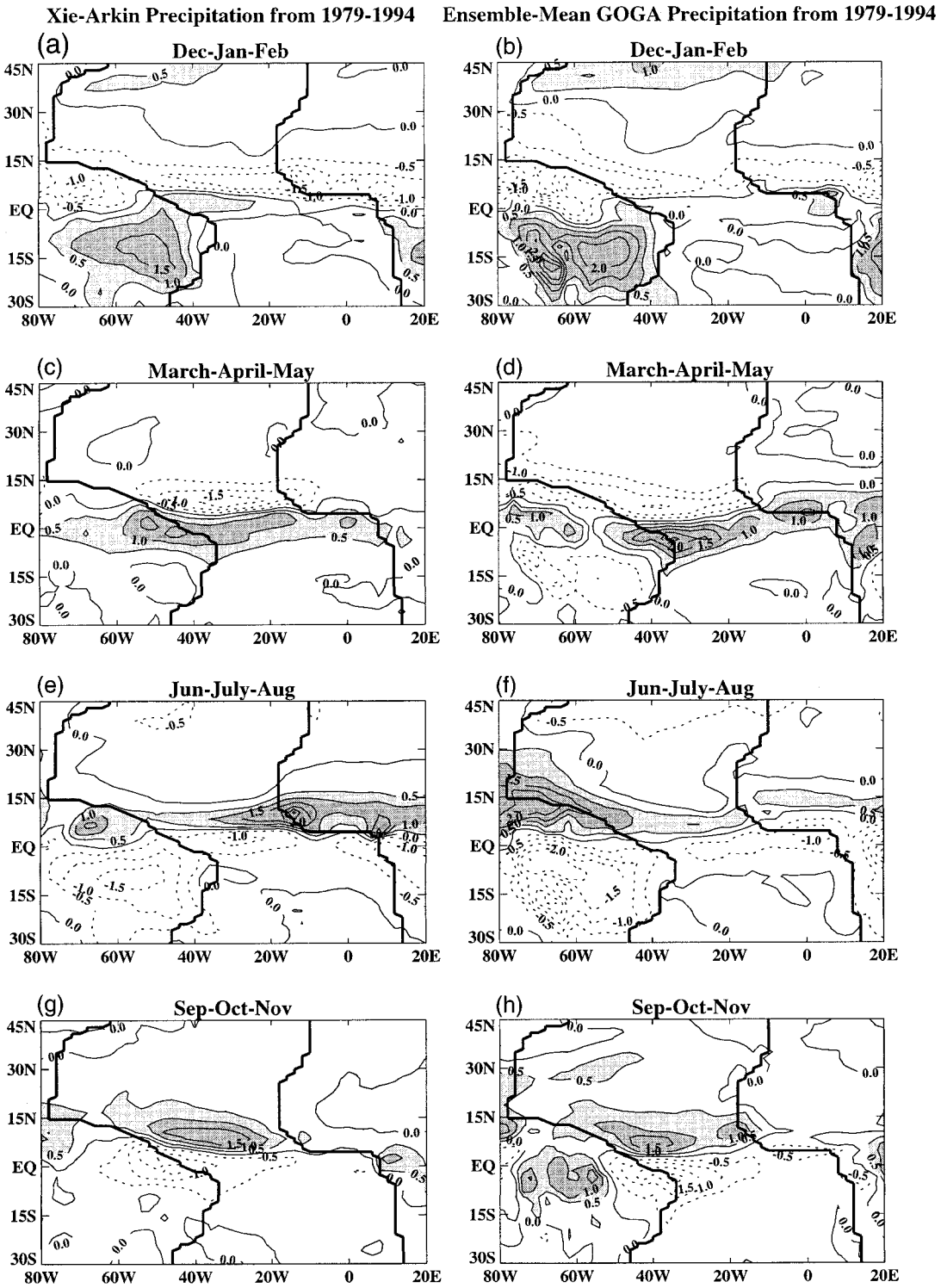

FIG. 3. Seasonal departures of observed (left panels) and simulated (right panels) precipitation from the annual means. The contour interval in all the figures is 0.5 m yr^{-1}.

of the variability is unrelated to the SST forcing in time even though it has well-defined spatial structures. The external part is often regarded as the ''signal'' because this part of the variability relates to changes in the oceans. Identifying the external part of atmospheric variability is crucial to the understanding of ocean–atmosphere interactions in the coupled system. However, it is also a challenging task because the forced response is often weak compared to the internal atmospheric variability, and the forced signal is highly contaminated by the noise.

Ensemble averaging can reduce the noise influences on the signal. If the ensemble size is sufficiently large (infinite, theoretically speaking), then the ensemble means represent the true forced response of the atmosphere to SST. In practice, however, the ensemble size is normally too small to accurately represent the forced response via simple ensemble averaging. In this case, the signal presented by the ensemble mean is contaminated by the internal variability of the atmosphere. Extra care must be taken to separate the forced response from the internal atmospheric variability. The key issue is how to maximize the signal-to-noise ratio based on a finite number of ensembles of model integrations.

To illustrate this point further, we constructed a meridional wind stress index by averaging the anomalies along an equatorial strip between 6°S and 6°N. Figure 4 depicts two indexes derived from ensemble averages of GOGA (Fig. 4a, dashed) and TAGA (Fig. 4b, dashed) runs along with the observed index derived from COADS (solid line). The shading indicates standard deviation about the ensemble mean computed from GOGA and TAGA experiments, respectively. From Fig. 4, it is evident that the ensemble means of the simulated cross-equatorial flows in both runs agree extremely well with each other. The simulated indexes also show a remarkable agreement with the observation, indicating that there is a forced response to local SST anomalies. However, there is a considerable spread among individual ensemble members in each experiment, even in the equatorial region, where the impact of internal atmospheric variability on forced response is expected to be weak. As one moves away from the deep Tropics toward higher latitudes, the spread within ensemble members increases and the ensemble mean based on a finite number of ensembles becomes more contaminated by the noise. A systematic treatment of the noise effect requires minimization of the influence of the noise in a global domain so that a pattern of forced response can be obtained.

a. Signal-to-noise maximizing EOF analysis

One approach to this problem is to apply the concept of optimal pattern detection to an ensemble of AGCM integrations in an attempt to maximize the signal-to-noise ratio in the direction of the forced response. Venzke et al. (1999) employed a signal-to-noise maximizing EOF analysis developed by Allen and Smith (1997) to extract the dominant forced atmospheric response in the North Atlantic sector. At the heart of this technique is a spatial prewhitening transformation that removes any spatial correlations in the internal atmospheric variability (i.e., noise) contained in the ensemble mean. This transformation ensures that spatial covariance in the ensemble average of the forced simulations is purely due to the forced response, since prewhitened atmospheric noise has no covariance between individual spatial components. Therefore, this technique isolates the dominant forced response better than other standard techniques. After the transformation, an EOF analysis of the ensemble average of the forced simulations isolates the forced response (in the prewhitened space) and its time evolution. It can be shown that this response time series has a maximum signal-to-noise ratio and exhibits the strongest coherence among individual ensemble members (see Fig. A2 for an illustration). The dominant patterns of the forced response can be obtained by regressing ensemble mean fields onto the time series. This is illustrated for the present case in the appendix. Venzke et al. (1999) demonstrated that the technique works quite well in identifying the dominant atmospheric response over the North Atlantic sector to the SST forcing from an ensemble of six GOGA runs of the Hadley Centre AGCM. Here, we apply this method to the tropical Atlantic Ocean in an attempt to extract the dominant atmospheric response to the local SST forcing.

The detailed description of the optimal detection algorithm and theoretical considerations can be found in Allen and Smith (1997) and Venzke et al. (1999). A brief outline of the technique is given in the appendix. To construct the prewhitening filter, one needs information about the internal atmospheric variability. In Venzke et al. (1999), the noise variance was estimated from the deviations of each ensemble member from the ensemble mean (i.e., within ensemble variability). In this study, since we have the output of the 145-yr ACYC run, which provides a good estimate of the internal variability of the model, we constructed the optimal filter based on the output of the ACYC simulation. In theory, the ACYC run should give a more accurate estimate of the true noise in the model than the deviations from the ensemble mean. In practice, we found that the results are not sensitive to the estimate of noise variance that is used. More discussion about this issue can be found in the appendix.

The actual construction of the optimal filter was based on the leading EOFs of the noise covariance derived from the 145-yr ACYC integration. To avoid using poorly sampled noise EOFs, it is necessary to limit the analysis space to that spanned by a certain number of noise EOFs. We followed the approach outlined in Venzke et al. (1999) to determine a truncation level of around 40. Therefore, a truncation level of 40 was used in our standard analyses. In comparison to Venzke et al. (1999), the truncation level we used is much higher. This could

be attributed to the fact that the signal we are seeking is confined to the Tropics while the noise is dominated by a NAO-like variability and is largely confined to Northern Hemisphere midlatitudes. Therefore, a large number of noise EOFs is needed to represent the forced response in the Tropics. As in Venzke et al. (1999), we have done extensive tests on the sensitivity of the results to different truncation levels and found that the results are stable between truncation levels 30–50. More discussion on the sensitivity of truncation levels and its effect on the signal-to-noise ratio are provided in the appendix. The results presented below were based on a prewhitening filter constructed using the first 40 leading EOFs of the noise covariance from the ACYC run.

b. Dominant forced responses

Figure 5 shows the dominant forced responses from the GOGA, TOGA, and TAGA experiments, respectively. Seasonally averaged wind stress and surface heat flux anomalies were used. The optimal detection method was operated simultaneously on zonal wind stress τ^x, meridional wind stress τ^y, and surface heat flux Q, that is, all three fields were simultaneously prewhitened. Prior to prewhitening, τ^x, τ^y, and Q were normalized by a spatially averaged standard deviation that corresponds to each of the three variables. We have also applied the method to individual variables and obtained essentially the same results. The SST patterns in Fig. 5 were obtained by regressing the SST anomalies in each experiment onto the corresponding time series of the dominant forced response (Fig. 5, bottom). It is evident that the responses in all three cases show a very similar pattern, which is largely confined within the Tropics. The correlations among the three time series of the forced responses are greater than 0.8. A decadal variation at 10–12-yr timescale is noted, similar to that found in the index of cross-equatorial SST gradient (Servain 1991; Mehta 1998). The dotted lines in the bottom panels of Fig. 5 represent the index of cross-equatorial SST gradient defined as the difference between the SST anomalies averaged over 6°–24°N and those over 6°–24°S. The correlations between the time series of the dominant forced response and the SST gradient index are highly significant, ranging from 0.54 for the TOGA runs to 0.61 for the TAGA runs. In contrast, the correlation between these time series and the Niño-3 SST index is low (less than 0.2), suggesting that the response is largely driven by the local SST anomaly. In all three cases, there is a pronounced response in the cross-equatorial wind and associated changes in the southeast and northeast trades near the equator. Consistent with the surface wind pattern, there are large surface heat flux anomalies of opposite sign on each side of the equator. The regressed SST patterns exhibit a strong gradient near the equator. However, anomalies in the Northern Hemisphere are stronger than those in the Southern Hemisphere. Therefore, the interhemispheric SST anomalies do not form a perfect dipole pattern.

By comparing the patterns of SST and surface heat flux, it is evident that the two patterns are not identical. This means that positive feedback does not occur globally in the sense that the anomalous heat flux reinforces the whole SST forcing pattern everywhere in the tropical Atlantic. However, there is a region in the western tropical Atlantic where the surface heat flux does reinforce the interhemispheric SST anomalies, indicating a local positive feedback. Interestingly, this region of positive feedback coincides nicely with the western Atlantic warm pool where the warmest SSTs reside in the tropical Atlantic. Because of the warm SST, one anticipates that, in this region, a strong atmospheric convective activity occurs and that latent heat flux tends to dominate the surface heat flux variability. Therefore, the positive feedback mainly takes place between the wind-induced latent heat flux and SST. This is confirmed by analyzing different components of the surface heat fluxes in the following section.

In the upwelling region off the coast of west Saharan Africa, where cold SST persists, the heat flux anomaly tends to damp the SST anomalies, indicating a local negative feedback. Because of the cold SST condition, one anticipates that atmospheric convective activity is weak and the local SST anomaly does not influence the atmospheric circulation significantly. Consequently, the atmosphere and ocean are effectively decoupled in this region, which implies that the SST variability in this region is likely to be forced by the heat flux associated with internal atmospheric variability. It will be shown below that much of the surface heat flux variability in this region is induced by air–sea surface temperature differences.

Although the overall patterns of the dominant forced response in GOGA, TOGA, and TAGA experiments are similar, there are noticeable differences among them (Fig. 5). Overall, the difference between GOGA and TOGA is smaller than that between TAGA and GOGA or TOGA, suggesting that the extratropical influence on the tropical Atlantic variability is less significant than the remote influence of ENSO. In comparison with GOGA and TOGA, the dominant forced response in TAGA has larger amplitudes in surface wind and heat flux anomalies in the north tropical Atlantic. The regressed SST pattern also shows a stronger northern component, resulting in less of a dipole structure in TAGA than that in the other two cases. This suggests that ENSO has an important impact in the north tropical Atlantic region, which is discussed in more detail in the companion paper (Saravanan and Chang 2000).

In contrast to the leading signal-to-noise maximizing EOF, which largely exhibits an antisymmetric structure about the equator (Fig. 5), the second EOF reveals a pattern that bears a certain resemblance to the tropical atmospheric response to the El Niño–related SST anomaly in the Pacific (Fig. 6). In all three cases, there is a

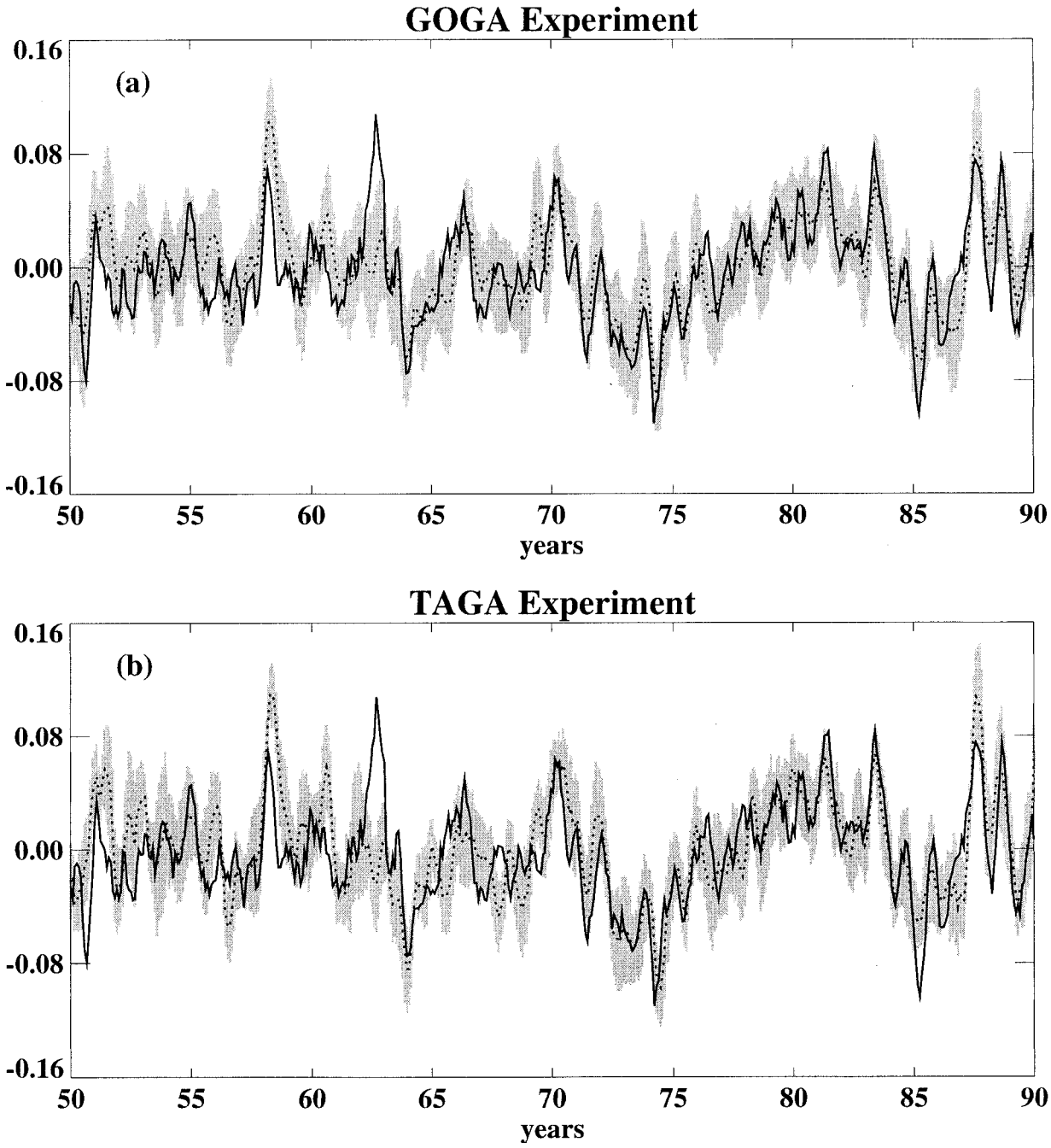

FIG. 4. Simulated (dashed) and observed (solid) meridional wind stress indexes for (a) GOGA experiment and (b) TAGA experiment. The shading in each panel shows standard deviation about the ensemble mean in each ensemble experiment.

relaxation of the easterly trades in the western equatorial region and a strong convergence of the meridional wind anomaly near the equator. Concurrent with these anomalous winds is a warming signal in the eastern equator region, as shown by the regressed SSTs (Fig. 6, top). The surface heat flux anomalies mainly act to dampen the SST anomalies. This configuration of wind and SST implies a positive dynamical feedback between the trade winds and SST, similar to the Bjerknes's ENSO mechanism (Bjerknes 1969). Zebiak (1993) suggests that this positive feedback may also operate in the equatorial Atlantic Ocean, giving rise to an ENSO-like, damped oscillatory mode. The fact that this ENSO-like pattern represents the second dominant forced response in the TAGA experiment as well as in the other two experiments gives some support to Zebiak's finding. Furthermore, the time series associated with this response shows largely interannual variability, but the correlation

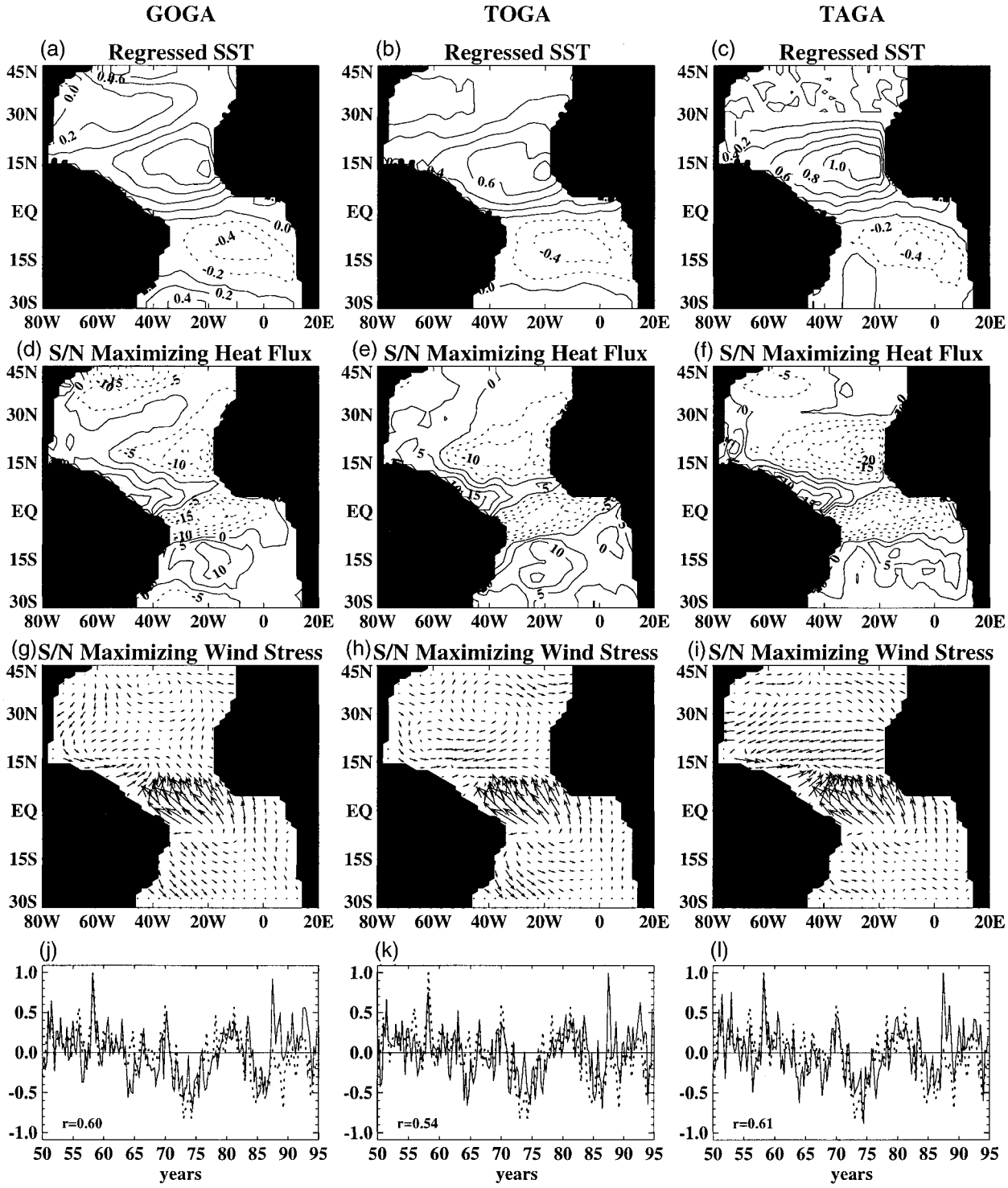

FIG. 5. The leading signal-to-noise maximizing EOFs from the (left column) GOGA, (middle column) TOGA, and (right column) TAGA experiment. (top) SST anomalies regressed onto the (bottom) time series of the dominant forced responses. (c)–(e) and (f)–(h). Spatial patterns of surface heat flux and surface wind stress vectors of the dominant forced response. (bottom) The time series of the dominant forced responses (solid) and the cross-equatorial SST gradient index (dashed). Correlations between the two time series are indicated in the lower left corner of each panel.

between the time series and Niño-3 SST index is rather low (less than 0.3), suggesting that this response may be an intrinsic mode to the tropical Atlantic. This result is also consistent with Zebiak's modeling results.

c. A further analysis of surface heat flux and precipitation anomaly

To dissect the feedback between the surface heat flux and SST, we made an attempt to evaluate the contribution from the different components of the net surface heat flux to the dominant heat flux pattern shown in Fig. 5. We divided the net flux into two parts: radiative flux and latent plus sensible flux. Since the latter is expected to contribute dominantly to the feedback process, we examined this part of the flux in further detail by splitting its total contribution into two parts: a flux anomaly F'_W due to changes in wind speed and a flux anomaly F'_T due to changes in air–sea temperature difference. Here, F'_W and F'_T were computed based on the simulated surface wind speed, W, and air–sea temperature difference, ΔT, using an approximate flux formula. Although these fluxes are not exact, the estimated total flux, F'_{est}, where $F'_{\text{est}} = F'_W + F'_T$, does provide a good estimate of the net flux anomaly in the Tropics. A detailed derivation and justification of the flux decompositions are described in the companion paper by Saravanan and Chang (2000).

Figure 7 shows the projections of the two anomalous flux components, F'_W and F'_T, along with the estimated total latent and sensible flux anomaly, F'_{est}, onto the time series of the dominant forced response (Fig. 5, bottom) for the GOGA and TAGA experiments (the result of the TOGA experiment is not shown because it is very similar to that of GOGA). The estimated latent and sensible heat fluxes, F'_{est} (Fig. 7, top), have clearly been successful in reproducing the patterns of the net surface heat fluxes (Fig. 5, middle panels), indicating that the estimated flux provides a good approximation for the net surface heat flux. The two components of the flux, F'_W and F'_T, show different contributions to the net flux. Within the deep Tropics, the wind-induced flux component, F'_W (Fig. 7, middle), shows a remarkably good agreement with the net flux anomaly in both GOGA and TAGA runs. The largest anomalies are found in the western Atlantic warm pool region, strongly suggesting that the wind-induced latent heat fluxes are most dominant and mainly responsible for the positive feedback in the warm SST region. This is consistent with the notion that the latent heat flux is a major contributing factor to surface heat flux variability in the warm pool region.

Outside the deep Tropics, the contribution from F'_W is substantially reduced and is generally much too weak to account for the net flux anomalies. The flux component due to the air–sea temperature difference, F'_T, appears to be a more important contributing factor to the net flux in these regions. This is particularly noticeable in the northeastern tropical Atlantic region off the coast of west Africa, where F'_T contributes to much of the negative anomaly in the net surface heat flux. Component F'_T also contributes to much of the positive net flux anomaly in the southern subtropical Atlantic. In contrast to the wind-induced flux, the flux due to the air–sea temperature difference largely plays a role in negative feedback in most parts of the tropical Atlantic Ocean. The only region where F'_T appears to contribute to the positive feedback is the northwestern tropical Atlantic. This contribution is noticeably stronger in the GOGA runs than in the TAGA runs, suggesting that the remote influence of ENSO may enhance the positive feedback in this region. Indeed, the analysis presented below finds that the ENSO's influence can explain a substantial portion of the positive feedback signal between the heat flux and SST in this region during the boreal spring. Saravanan and Chang (2000) take a more detailed look at the remote influence of ENSO.

To examine the effect of local SST anomalies on the precipitation, we regressed the seasonally averaged precipitation anomalies from GOGA and TAGA onto the corresponding time series of the dominant forced responses (Fig. 5j and l). The results are shown in Fig. 8. The patterns for GOGA and TAGA runs are again very similar. In both cases, the precipitation fields show a dipolelike pattern in the tropical Atlantic, akin to the leading EOF of the ensemble mean precipitation (not shown) and the regression of precipitation anomalies from TAGA onto a tropical Atlantic SST index (Saravanan and Chang 2000). This suggests that much of the simulated rainfall variability in the region is indeed driven by the local SST, which is in line with previous studies (Hastenrath 1990; Hastenrath and Greishar 1993; Graham 1994). In the companion paper (Saravanan and Chang 2000), we further examine local versus remote SST influences on the precipitation variability in the tropical Atlantic sector.

d. Seasonal dependence of the forced responses

To examine the seasonality of the forced response, we stratified the model data into four seasons—winter [December–February (DJF)], spring [March–May (MAM)], summer [June–August (JJA)] and fall [September–November (SON)]—and computed signal-to-noise maximizing EOFs for each season. Compared to the all-season analysis, the sample size is reduced by a factor of 4 for seasonally stratified data. Therefore, the truncation level must be carefully determined to avoid undersampling problems. For the results presented below, the truncation level for each season is individually determined for each experiment. Details are given in the appendix.

Figures 9 and 10 show the dominant forced patterns in different seasons for the GOGA and TAGA experiments, respectively. The responses of the TOGA experiment (not shown) bear a strong resemblance to those

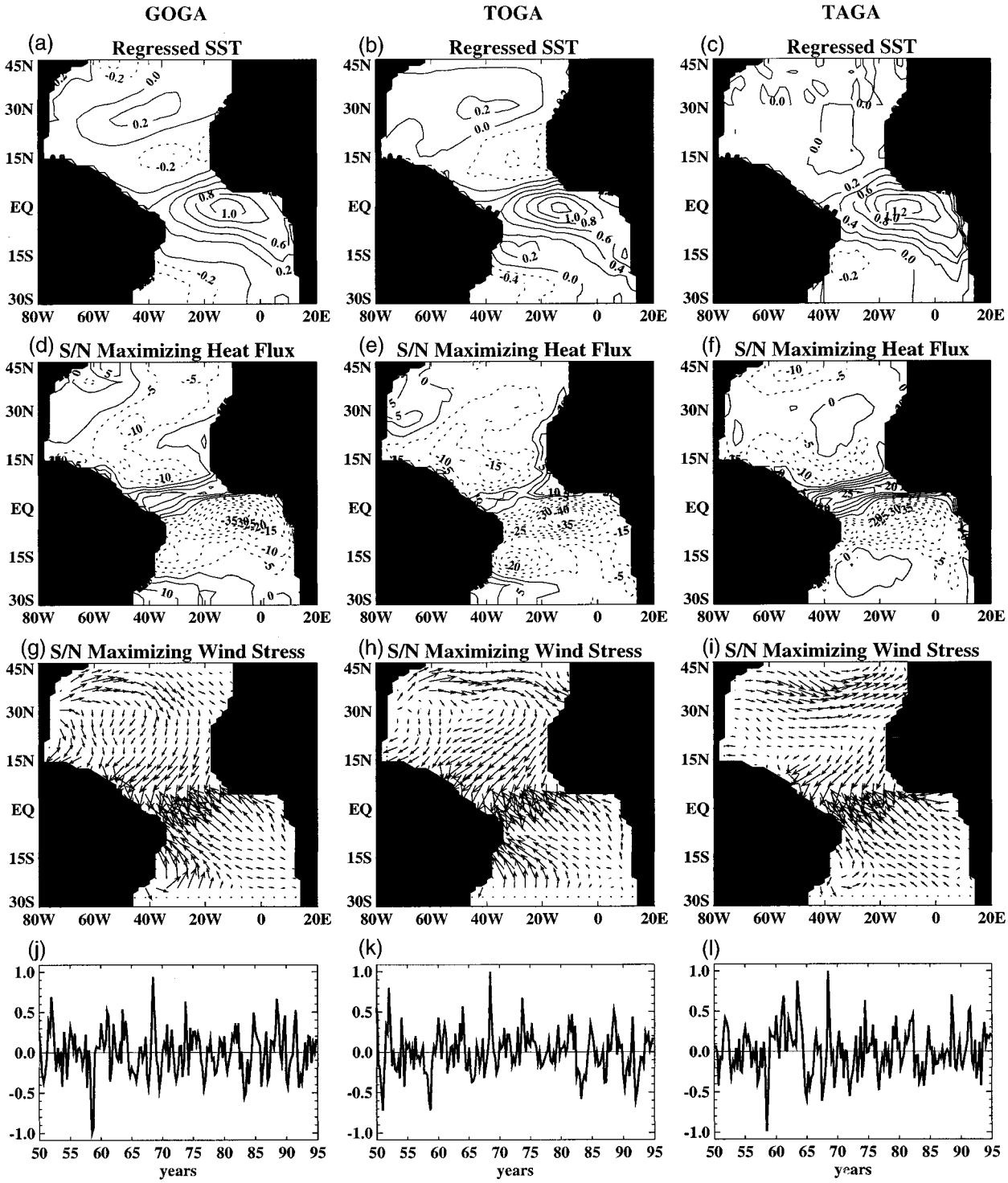

FIG. 6. Same as Fig. 5 except that these are the second leading signal-to-noise maximizing EOFs.

of GOGA, indicating that the dominant remote influence on the tropical Atlantic variability comes mainly from the tropical Pacific ENSO (Saravanan and Chang 2000). The most noticeable difference between the GOGA and TAGA experiments occurs in the boreal spring. During this season the GOGA response exhibits a large surface heat flux anomaly in the western tropical Atlantic and a strong cross-equatorial SST gradient, indicating a strong positive feedback. The TAGA experiment, on the other hand, shows a much reduced surface heat flux

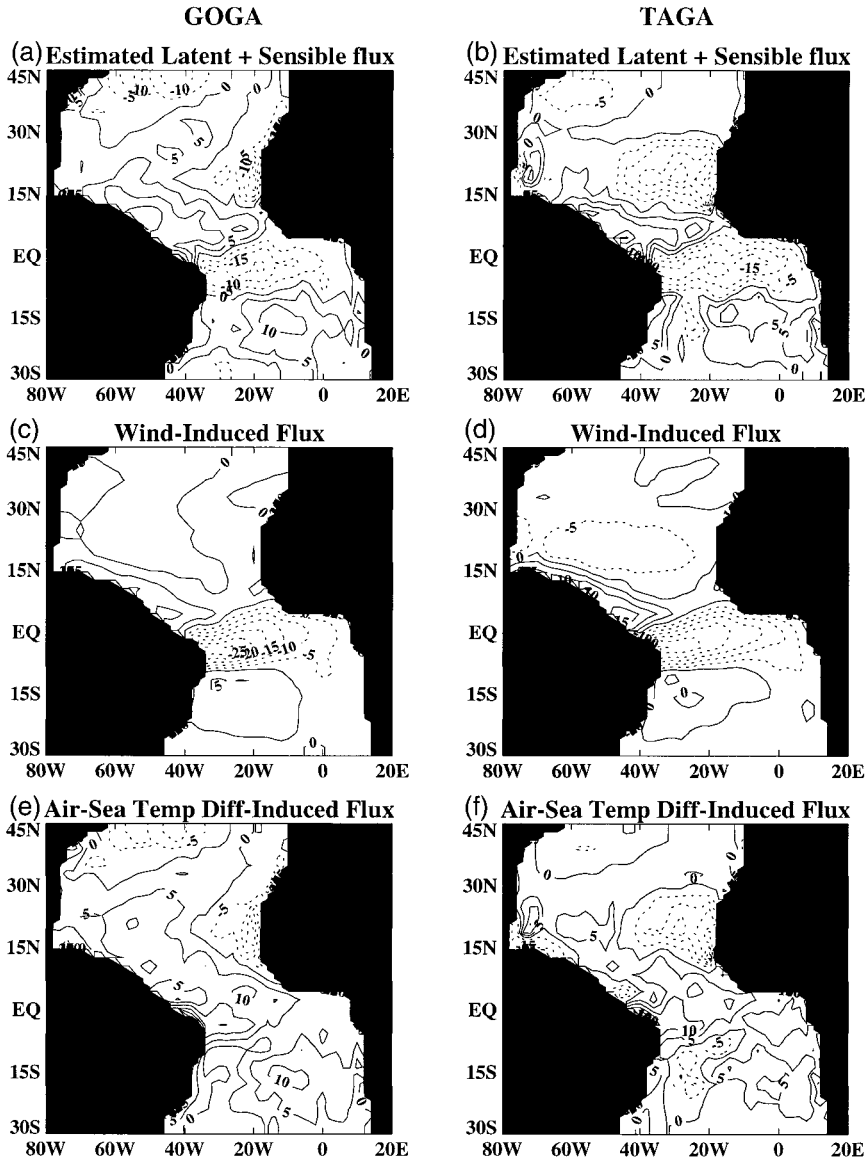

FIG. 7. Various components of the surface heat flux anomaly regressed onto the time series of the leading signal-to-noise maximizing EOFs from the (left) GOGA and (right) TAGA experiments (Fig. 5, bottom). (top) Estimated latent and sensible flux, $F'_{\text{est}} = F'_W + F'_T$. (middle) Flux components due to changes in wind speed, F'_W. (bottom) Flux components due to changes in the air–sea temperature difference, F'_T.

anomaly and SST gradient, although the flux and SST patterns still constitute a positive feedback in the tropical Atlantic warm pool region. This result indicates that the Pacific ENSO exerts its strongest remote influence on the tropical Atlantic variability during the boreal spring and contributes to much of the positive feedback in the tropical Atlantic in this season. This finding is consistent with other recent studies by Enfield and Mayer (1997), Harrison and Larkin (1998), and Giannini et al. (1998) in that the strongest ENSO influence occurs in the north tropical Atlantic during the boreal spring. Outside the Tropics, there is also a noticeable ENSO influence along the Gulf Stream region, where a large surface heat flux anomaly is found in the GOGA runs but not in the TAGA runs. Anomalous wind patterns are also quite different between the two runs. Harrison and Larkin (1998) noted a similar ENSO influence in the SST anomaly.

The remote influences in the other seasons appear to be considerably weaker than those during the boreal spring. The patterns of dominant forced responses in the GOGA and TAGA experiments show a great deal of similarity. In particular, the winter season responses in both experiments show similar positive feedback pat-

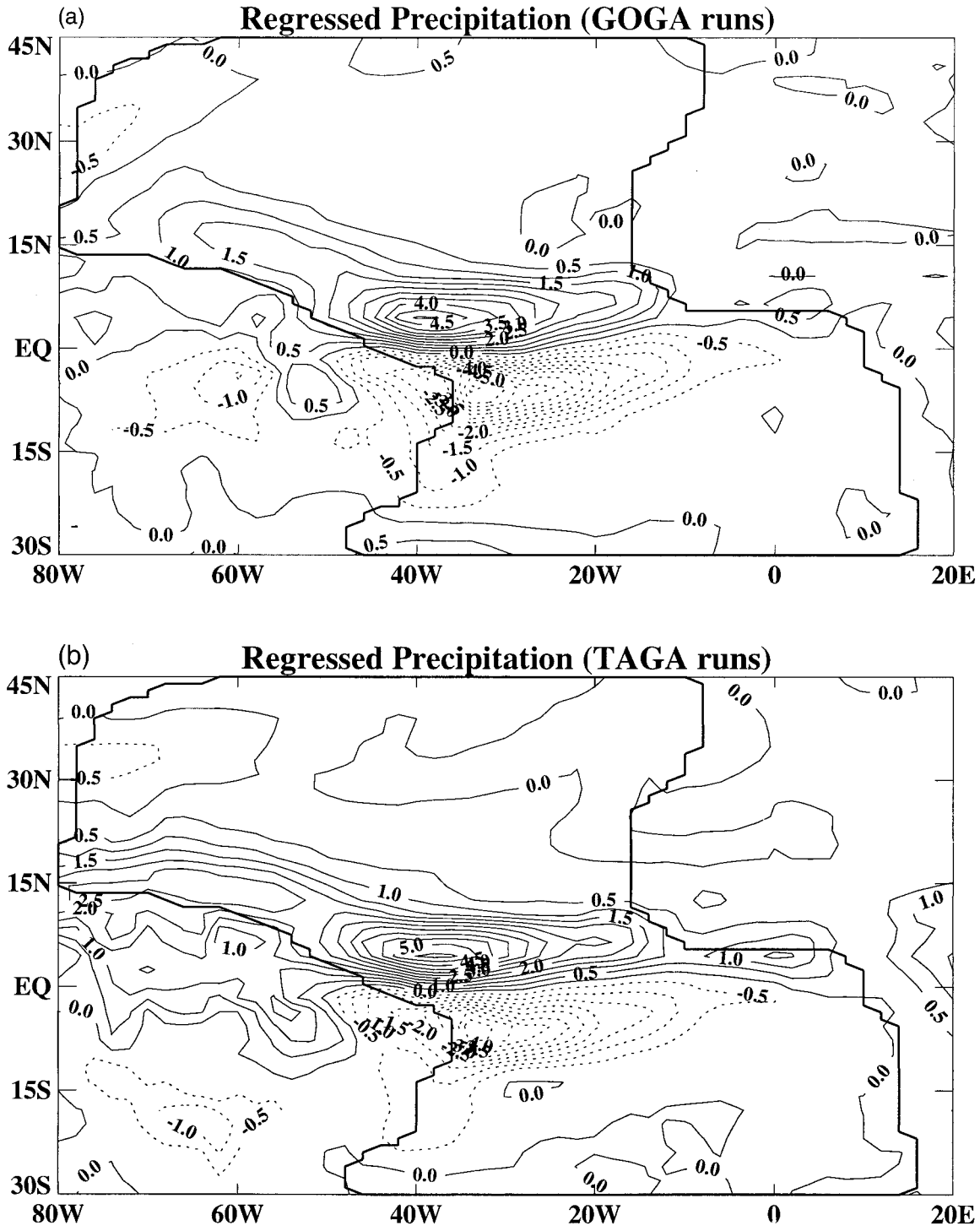

FIG. 8. Precipitation anomaly regressed onto the time series of the dominant forced responses, (Fig. 5, bottom) from GOGA and TAGA experiments.

terns between surface heat flux and SST anomalies in the western tropical Atlantic. During the Northern Hemisphere summer, there are large surface heat flux anomalies forming in the southern deep Tropics. Overall, the tropical responses during winter, spring, and summer share many common features to the leading signal-to-noise maximizing EOF in the all-season case (Fig. 5). The all-season responses are particularly similar to the winter patterns, suggesting that year-to-year variability in the tropical Atlantic is dominated by the

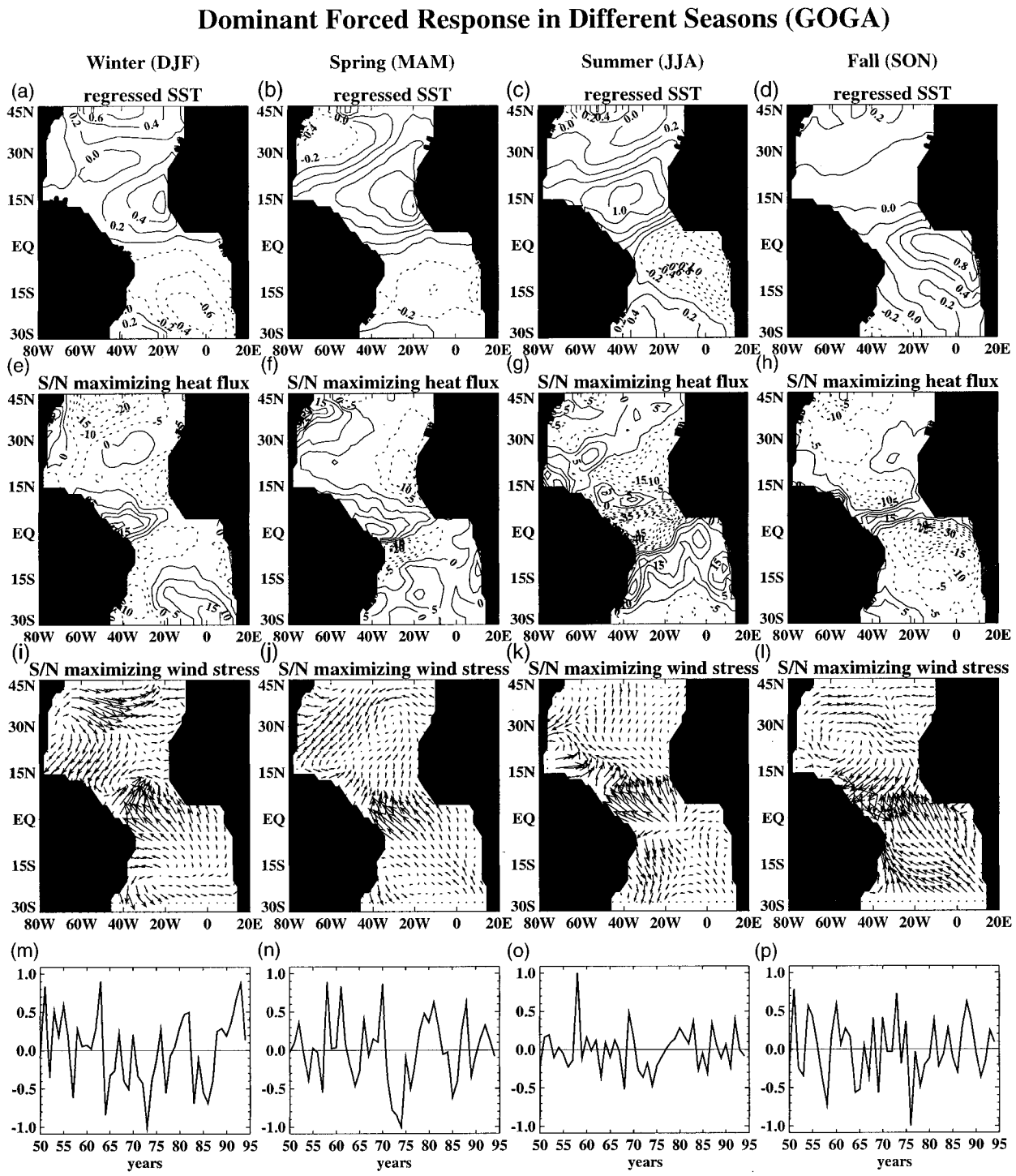

FIG. 9. Dominant forced responses in different seasons from the GOGA experiment. The panels from left to right show the forced responses in winter (DJF), spring (MAM), summer (JJA), and fall (SON), respectively.

winter season anomalies. In contrast, the fall season response reveals a somewhat different pattern. The response in this season shows an ENSO-like structure akin to the second dominant signal-to-noise maximizing EOF in the all-season case (Fig. 6). The positive feedback between surface heat flux and SST appears to be the weakest while the Bjerknes-type dynamics feedback may be the strongest. This suggests that much of the ENSO-like variability in the tropical Atlantic may be dominated by the fall season anomalies.

6. Summary and discussion

By analyzing the output of three ensembles of multidecadal NCAR CCM3 integrations, a systematic assessment of the effect of tropical Atlantic SSTs on atmospheric circulation is made. A signal-to-noise maximizing EOF analysis is employed to isolate the dominant forced response from the internal atmospheric variability. The principal findings of this study are as follows.

1) The local SST anomalies do exert a significant influence on the atmospheric circulation in the tropical Atlantic sector. Of particular importance is the variability of the cross-equatorial SST gradient. The dominant forced response in the tropical Atlantic sector appears to be driven by the SST gradient. A 10–12-yr decadal signal is noted in the time series of the dominant forced response.
2) There is modeling evidence that the positive feedback between wind-induced latent heat flux and SST operates in the tropical Atlantic Ocean, as hypothesized by Chang et al. (1997) and Carton et al. (1996). However, this feedback does not operate globally in the tropical Atlantic. It occurs primarily in the western tropical Atlantic warm pool region where latent heat flux appears to be dominant.
3) A negative feedback between surface heat flux and SST is found in the northeastern tropical Atlantic off the coast of west Saharan Africa, where SST is generally cold due to local upwelling. It suggests that the SST variability in this region is primarily forced by the atmosphere.
4) An ENSO-like response is also identified in the equatorial Atlantic. It is represented by the second dominant signal-to-noise maximizing EOF. The associated time series exhibits interannual variability. It implies that the Bjerknes dynamical feedback between equatorial trades and SST may play some role in interannual variability of equatorial Atlantic SST, which is in line with the modeling study of Zebiak (1993).
5) The dominant forced responses exhibit seasonal dependence. The feedback between surface heat flux and SST appears to be strongest during the boreal winter and spring, and the Bjerknes-type dynamical feedback may be most active during the boreal fall. The winter–spring anomalies contribute to much of the year-to-year variability in the north–south shift of the ITCZ, whereas the fall anomalies dominate much of the ENSO-like variability in the tropical Atlantic.
6) A significant remote influence of the Pacific ENSO on the tropical Atlantic variability is noted. The effect of ENSO is strongest during the boreal spring, and much of its influence is found in the northern tropical Atlantic. The remote ENSO influence adds substantially to the positive feedback in the north tropical Atlantic. Saravanan and Chang (2000) discuss further details of the remote influence of ENSO.

The modeling results presented are generally consistent with the notion that the tropical Atlantic variability stems from two major sources: local SST anomalies and remote influence from ENSO-related SST anomalies in the tropical Pacific.

It is worth further commenting on the implications of the positive and negative feedbacks to the SST evolution in the tropical Atlantic. As noted earlier, the negative feedback in the northeastern tropical Atlantic implies that the SST variability in that region directly results from atmospheric forcing. Because the SST anomalies have little effect on the atmospheric circulation in this region, the surface heat flux anomalies are most likely to be generated by internal atmospheric variability such as the NAO. Indeed, recent ocean modeling studies by Visbeck et al. (1998) and Chang et al. (2000) show that large SST anomalies can be generated by an NAO-like forcing off the coast of west Saharan Africa. Once the anomalies form, the positive heat flux feedback in the western tropical Atlantic warm pool tends to strengthen the SST anomalies and causes them to move equatorward and westward toward the coast of northeast Brazil. This effect will give rise to an apparent westward ''propagation'' of the SST anomalies. This time-evolving SST pattern in the north tropical Atlantic has been identified by Mehta (1998) as an energetic mode of the decadal SST variations based on a century-long observed SST analysis. According to Mehta (1998), the SST anomalies first enter the north tropical Atlantic along the eastern boundary of the basin, then travel equatorward and westward as they gain strength. The anomalies reside in the western tropical Atlantic for several years before moving northward along the western boundary. This result is also consistent with a hybrid coupled model study by Chang et al. (2000) in which it is shown that the local heat flux feedback can significantly enhance both the amplitude and persistence of the NAO-generated SST anomalies in the deep Tropics.

Although the present study provides some indications for local air–sea interactions in the tropical Atlantic, the extent to which the ocean–atmosphere coupling can influence tropical Atlantic variability remains to be explored. The results shown here do not represent a complete picture of feedback processes because they only take into consideration the atmospheric response to SST forcing and do not include oceanic processes. In the real coupled system, certain oceanic processes may act in concert with atmospheric processes to enhance feedback whereas other processes may work against atmospheric processes to suppress the positive feedback. For example, while the feedback between wind-induced heat flux and SST operates in the western tropical Atlantic warm pool region, the anomalous Ekman flow driven by a northward cross-equatorial wind anomaly can enhance the feedback by intensifying upwelling to the south of the equator (Chang and Philander 1994). A comprehensive understanding of the role of air–sea in-

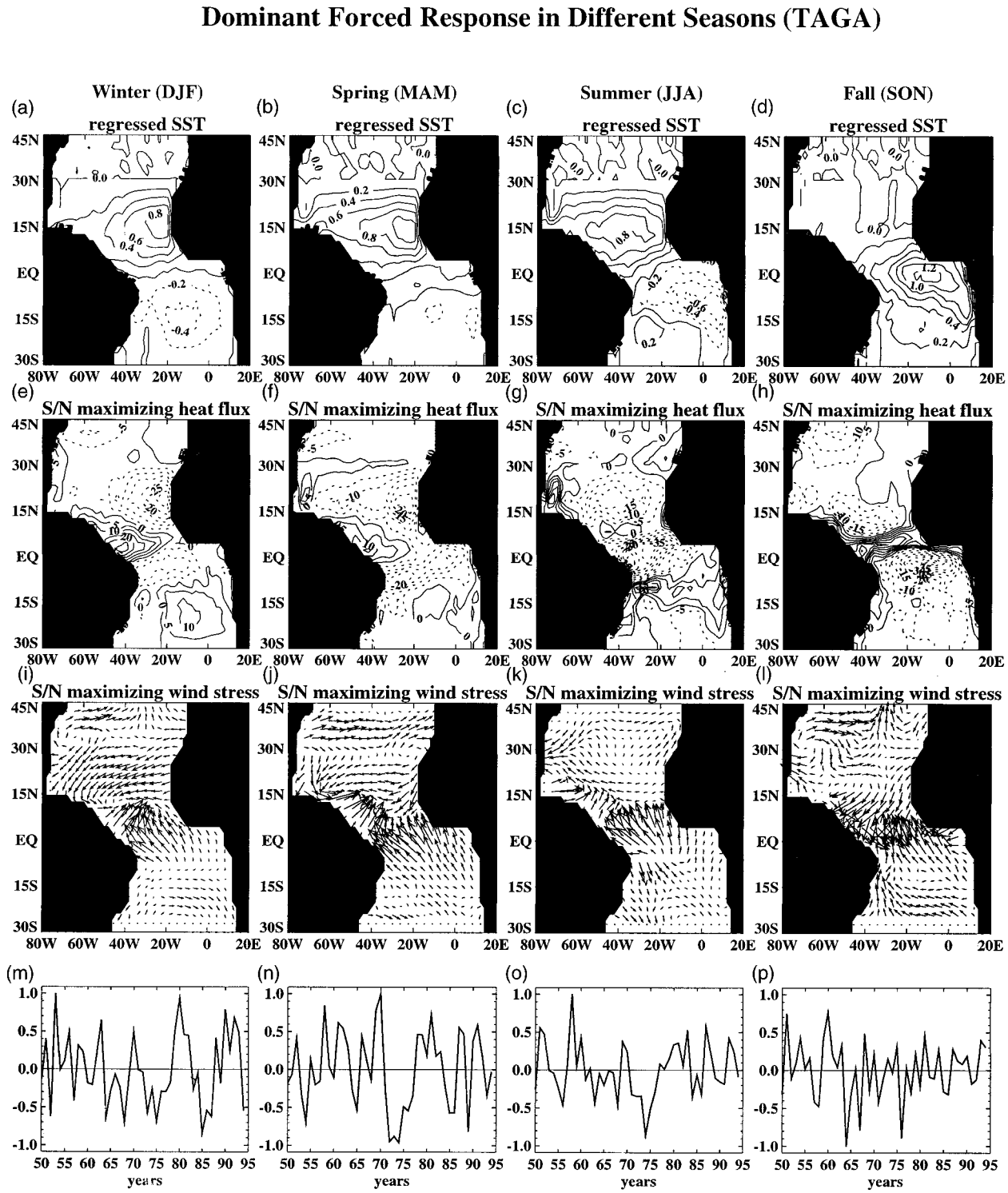

FIG. 10. Same as Fig. 9 but for the TAGA experiment.

teractions in tropical Atlantic variability requires the use of a hierarchy of coupled models.

Some recent studies (Robertson et al. 1998; Rajagopalan et al. 1998) indicate that tropical Atlantic SST variability potentially has an influence on extratropical climate variability such as the NAO. The TAGA experiment could shed light on this issue. We have not conducted a thorough investigation on this issue because

the primary interests of this study are in the local atmospheric response to SST forcing in the tropical Atlantic. There are, however, some indications of tropical Atlantic SST influence on extratropical atmospheric circulation in the dominant forced responses (Fig. 5) from the TAGA experiment, although the signal is weak. We plan to analyze this signal in more detail in the context of potential predictability associated with tropical Atlantic SST anomalies.

The atmospheric response to local SSTs and the associated feedback processes in the tropical Atlantic appear to be closely related to the north–south movement of the ITCZ. Therefore, it is crucial that the AGCMs well represent and resolve the dynamical and thermodynamical processes that govern the ITCZ. Although at the current resolution, T42, the CCM3 captures the major features of the tropical circulation in the Atlantic sector, the model is far from perfect. Further studies are needed to examine how sensitive the results presented here are to changes in the model resolution and physics. To this end, it is useful to compare the CCM3 simulations with other AGCM simulations in the tropical Atlantic sector.

There are some general concerns about diagnosing surface heat fluxes in an AGCM forced with specified SST, that is, Atmospheric Model Intercomparison Project (AMIP)–type runs. Barsugli and Battisti (1998) show that AMIP-type runs could produce erroneous surface heat fluxes because of an infinite heat reservoir at the lower boundary. Therefore, this type of integration could be problematic for understanding the feedbacks acting to produce low-frequency variability in the climate system. To address partially this concern, we have also performed a similar analysis on the output of a 99-yr integration of CCM3 coupled to an ocean mixed-layer model. The result reveals a tropical circulation pattern very similar to the dominant forced response found in the GOGA, TOGA, and TAGA experiments. Consistent with the forced response in these experiments, it also shows a positive feedback relation between the surface heat flux and SST anomalies in the tropical Atlantic region. There are, however, differences in the flux anomalies between the coupled mixed-layer and AMIP experiments outside the Tropics. Further studies are needed to understand the dynamic differences between the two types of simulations.

Acknowledgments. We would like to thank Dr. Myles Allen for the very helpful discussions about the signal-to-noise maximizing EOF analysis. We would like to acknowledge the contribution of Jeff Lee, who carried out the AGCM integrations at NCAR. This work is supported by NOAA's Global Climate Change Program under Grants NA76GP0454 and NA86GP0303. P.C. is also supported by the NSF Young Investigator Award. GCH is supported by the Alexander von Humboldt Foundation, the National Science Foundation (Grant ATM-9707069), and JISAO.

APPENDIX

Signal-to-Noise Maximizing EOF Analysis

a. Outline of the method

The method of constructing signal-to-noise maximizing EOFs is described in detail by Venzke et al. (1999) with an algorithm. To make this paper self-contained, we give a brief outline of the technique. Some of the technical issues concerning the truncation level and other problems are also discussed.

An ensemble average of a small number of AGCM integrations forced with the same SST boundary conditions consists of the atmospheric signal forced by SST and atmospheric noise due to internal variability:

$$\mathbf{X}_M = \frac{\sum_{k=1}^{K} \mathbf{X}_k}{K} = \mathbf{X}_F + \frac{\sum_{k=1}^{K} \mathbf{X}_N^{(k)}}{K}, \tag{A1}$$

where $\mathbf{X}_M$ is the data matrix of the total response of the kth ensemble member, $\mathbf{X}_F$ is the true forced response, and $\mathbf{X}_N^{(k)}$ is the atmospheric noise (or internal variability) in the kth ensemble integration. The total ensemble size is K, which is a relatively small number.

If a standard EOF technique is applied, the estimated spatial covariance of the ensemble mean, $\mathbf{C}_M$, will consist of a sum of the covariance of the signal $\mathbf{C}_F$ and the noise $\mathbf{C}_N$, that is,

$$\mathbf{C}_M = \mathbf{C}_F + \frac{\mathbf{C}_N}{K}. \tag{A2}$$

For small ensemble sizes, the eigenvalues of $\mathbf{C}_M$ will consist of both signal and noise, and a standard EOF technique will not be able to separate the forced response from noise. Therefore, a procedure is needed to reduce the noise contamination in the ensemble mean. This can be done by prewhitening the atmospheric noise to remove its spatial coherence. Mathematically, this is equivalent to diagonalizing the noise covariance matrix:

$$\mathbf{F}^{\mathrm{T}}\mathbf{C}_N\mathbf{F} = K\mathbf{I} \tag{A3}$$

where $\mathbf{F}$ is a prewhitening filter. If this prewhitening transformation [eq. (A3)] is applied to (A2), the eigenvectors of the prewhitened $\mathbf{C}_M$ will be identical to those of the prewhitened $\mathbf{C}_F$ (since the prewhitened $\mathbf{C}_N$ is diagonal), yielding an estimate of the dominant forced patterns. The transform

$$\mathbf{X}'_M = \mathbf{F}^{\mathrm{T}}\mathbf{X}_M = \sqrt{K}(\mathbf{\Lambda})_N^{-1}\mathbf{E}_N^{\mathrm{T}}\mathbf{X}_M \tag{A4}$$

yields the required diagonalization of $\mathbf{C}_M$ (Venzke et al. 1999). Here, $\mathbf{E}_N$ is the matrix of the eigenvectors of $\mathbf{C}_N$ and $\mathbf{\Lambda}_N$ is the diagonal matrix of the square root of the eigenvalues of $\mathbf{C}_N$. Note that $\mathbf{F}$ is completely determined by the noise covariance $\mathbf{C}_N$. In our case, $\mathbf{C}_N$ is estimated based on the ACYC simulation, because this simulation should contain only atmospheric internal variability. The ACYC run was integrated for 145 yr, which, for seasonally averaged data, generates 145 $\times$ 4 samples.

This sample size is too small to get a reliable estimate of the high-ranking eigenvectors of the covariance $\mathbf{C}_N$. Therefore, only a limited number, J, of eigenvectors in $\mathbf{E}_N = (\mathbf{e}_1 \cdots \mathbf{e}_j)$ and eigenvalues in $\mathbf{\Lambda}_N$ should be used. Otherwise, $\mathbf{C}_N$ will be singular and the high eigenvalues will be severely underestimated, yielding very high values in (A4). The choice of the truncation level J is further discussed.

Once the ensemble mean fields are prewhitened, an EOF analysis is performed on the transformed data matrix, $\mathbf{X}'_M$. This yields eigenvectors $\mathbf{e}'_1, \ldots, \mathbf{e}'_j$ and principal components $\mathrm{pc}_1(t), \ldots, \mathrm{pc}_j(t)$. It can be shown that $\mathrm{pc}_1(t)$ represents the time evolution of the most dominant forced response that has the maximum signal-to-noise ratio. The spatial response pattern **e** in the original space can be obtained by regressing $\mathrm{pc}_1(t)$ onto the ensemble mean, $\mathbf{X}_M$ (Venzke et al. 1999).

b. Technical details

The truncation level, J, should be high enough to yield a good representation of the forced signal pattern via the EOFs of the noise but low enough to avoid sampling problems. The ratio of the cumulative variance $r = \sum_{j=1}^{J} \sigma_M^{(j)^2} / [(1/K)\sigma_N^{(j)^2}]$ as a function of truncation J gives a useful indicator for a proper truncation (Venzke et al. 1999). Here, $\sigma_M^{(j)^2}$ denotes the variance of the jth noise EOF pattern in the ensemble mean $\mathbf{X}_M$ and $\sigma_N^{(j)^2}$ is that of the noise $\mathbf{X}_N$. The variable r provides information about the relative contribution of the noise EOFs to the forced atmospheric response and to the internal variability. Figure A1 shows an example for the GOGA experiment. It shows that after about 30–40 EOFs, the variance ratio appears to saturate (although not completely), and the higher ranking EOFs contribute little to the signal, suggesting a truncation level between 30 and 40. As a rule of thumb, we demand that the minimum number of samples per truncation level is greater than five. Given the 145×4 samples we have available for the seasonal data, 40 leading EOFs should be well sampled.

Figure A2a illustrates the sensitivity of $\mathrm{pc}_1(t)$ to changes in truncation level using $J = 30$, 40, and 50. It is evident that the result is quite stable between truncation levels 30 and 50. To demonstrate that $\mathrm{pc}_1(t)$ indeed captures the forced signal, Fig. A2b displays the projections of an individual ensemble member of the GOGA experiment onto the optimal filter pattern, $\hat{\mathbf{e}}_1 = \mathbf{F}\mathbf{e}'_1$, along with the time series, pc_1, of the dominant forced response pattern, **e**. The projected time series covary nicely with pc_1, indicating that pc_1 indeed represents a forced signal that is common to all the ensemble members. Note that the optimal filter pattern $\hat{\mathbf{e}}_1$ and the dominant forced pattern **e** are not identical. This can be understood elegantly as the contravariant signal-to-noise filter pattern to the covariant physical pattern (see Hasselmann 1979). Physically, the pattern that yields the optimal time series of the forced response is one that down-weights the influence of the noise on the pattern.

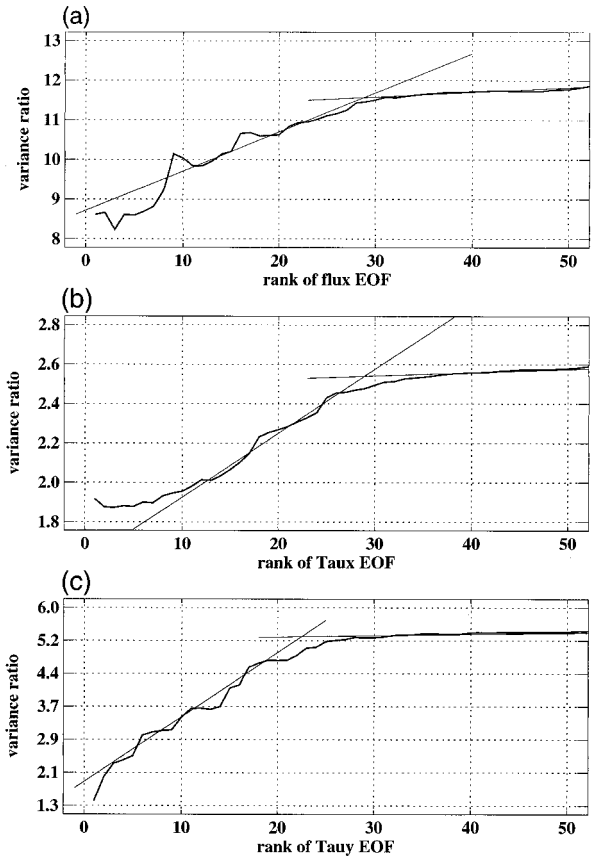

FIG. A1. The ratio of the cumulative variance r as a function of truncation, J. Here, r is defined in the appendix and provides information about the relative contribution of the noise EOFs to the forced atmospheric response and to the internal variability.

Many sensitivity tests have been performed to assure that the results are stable and do not depend on technical details of the method, such as the truncation level, data averaging (monthly, seasonal, and yearly data), and estimation of noise covariance, $\mathbf{C}_N$ (based on ACYC simulation or within ensemble variability). The results for the seasonal and monthly mean data are remarkably stable. The case of individual seasons and annual mean data shows some sensitivity for the choice of truncation level. This is likely due to uncertainty associated with undersampling. Therefore, the results for individual seasons need to be treated with some care. To assess the sensitivity to choice of truncation level, we varied the truncation level for each individual season from 22 to 40 and chose the truncation at which the results stabilizes and change little when moving to the next few higher truncation levels. The truncation levels for DJF, MAM, JJA, and SON were 36, 28, 28, and 26, respectively, for the GOGA runs and 28, 28, 28, and 26, respectively, for the TAGA runs. All the truncation levels,

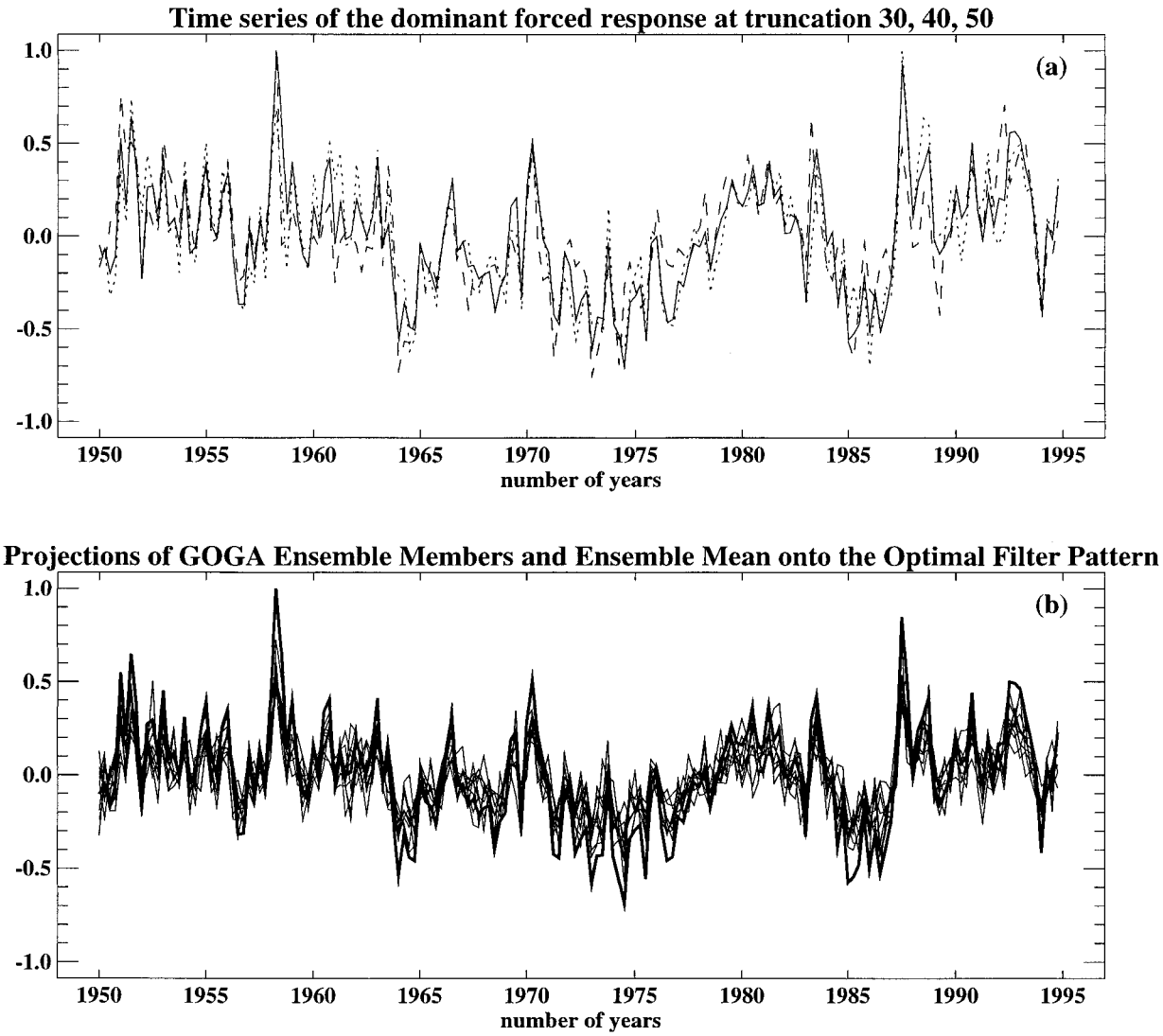

FIG. A2. (a) Time series of the dominant forced response at truncation level 30 (dashed), 40 (solid), and 50 (dotted) from the GOGA experiment. (b) Time series of the dominant forced response (truncation level 40) superimposed on the projections of 10 GOGA ensemble members onto the optimal filter pattern defined in the appendix.

except for the DJF season in the GOGA runs, satisfy the requirement of a minimum of five samples per truncation. To assure that the result is not significantly affected by the undersampling problem, we used the within-ensemble variability to construct the prewhitening filter and then repeated the signal-to-noise maximizing EOF analysis. Because there are 10 ensemble members in the GOGA experiments, the sample size using the within-ensemble noise estimate is increased by more than a factor of 2, reducing the uncertainties associated with undersampling. We found that response patterns and time series obtained using both noise estimates are very similar. The stability of the results and the fact that the results are consistent with those for all seasons give some confidence in the seasonal results.

REFERENCES

Allen, M. R., and L. A. Smith, 1997: Optimal filtering in singular spectrum analysis. *Phys. Lett.*, **234,** 419–428.

Barsugli, J. J., and D. S. Battisti, 1998: The basic effects of atmosphere–ocean thermal coupling on midlatitude variability. *J. Atmos. Sci.*, **55,** 477–493.

Bjerknes, J., 1969: Atmospheric teleconnections from the equatorial Pacific. *Mon. Wea. Rev.*, **97,** 163–172.

Bonan, G. B., 1998: The land surface climatology of the NCAR Land Surface Model coupled to the NCAR Community Climate Model. *J. Climate*, **11,** 1307–1326.

Carton, J. A., X. Cao, B. S. Giese, and A. M. da Silva, 1996: Decadal and interannual SST variability in the tropical Atlantic. *J. Phys. Oceanogr.*, **26,** 1165–1175.

Chang, P., and S. G. Philander, 1994: A coupled ocean–atmosphere instability of relevance to the seasonal cycle. *J. Atmos. Sci.*, **51,** 3627–3648.

——, L. Ji, and H. Li, 1997: A decadal climate variation in the tropical Atlantic Ocean from thermodynamic air–sea interactions. *Nature,* **385,** 516–518.

——, ——, and R. Saravanan, 2000: A hybrid coupled model study of tropical Atlantic variability. *J. Climate,* in press.

da Silva, A., A. C. Young, and S. Levitus, 1994: *Algorithms and Procedures.* Vol. 1, *Atlas of Surface Marine Data 1994,* NOAA Atlas NESDIS 6, 83 pp.

Davies, J. R., D. P. Rowell, and C. K. Folland, 1997: North Atlantic and European seasonal predictability using an ensemble of multi-decadal AGCM simulations. *Int. J. Climatol.,* **17,** 1263–1284.

Delworth, T. L., and V. M. Mehta, 1998: Simulated interannual to decadal variability in the tropical–subtropical North Atlantic. *Geophys. Res. Lett.,* **25,** 2825–2828.

Dommenget, D., and M. Latif, 2000: Interannual to decadal variability in the tropical Atlantic. *J. Climate,* **13,** 777–792.

Enfield, D. B., 1996: Relationships of inter-American rainfall to tropical Atlantic and Pacific SST variability. *Geophys. Res. Lett.,* **23,** 3305–3308.

——, and D. A. Mayer, 1997: Tropical Atlantic SST variability and its relation to El Niño–Southern Oscillation. *J. Geophys. Res.,* **102,** 929–945.

Folland, C., T. Palmer, and D. Parker, 1986: Sahel rainfall and worldwide sea temperatures: 1901–85. *Nature,* **320,** 602–606.

Giannini, A., Y. Kushnir, and M. A. Cane, 1998: Interannual variability of Caribbean rainfall, ENSO, and the Atlantic Ocean. *J. Climate,* **13,** 297–311.

Graham, N., 1994: Experimental predictions of wet season precipitation in Northeastern Brazil. *Proc. 18th Annual Climate Diagnostics Workshop,* Boulder, CO, NOAA, CAC, 397 pp.

Harrison, D. E., and N. K. Larkin, 1998: El Niño–Southern Oscillation: Sea surface temperature and wind anomalies, 1964–1993. *Rev. Geophys.,* **36** (3), 353–399.

Harzallah, A., J. O. Rocha De Aragao, and R. Sadourny, 1996: Interannual rainfall variability in North-East Brazil: Observation and model simulation. *Int. J. Climatol.,* **16,** 861–878.

Hasselmann, K., 1979: On the signal-to-noise problem in atmospheric response studies. *Meteorology over the Tropical Oceans,* D. B Shaw, Ed., Roy. Meteor. Soc., 251–259.

Hastenrath, S., 1976: Variations in low-latitude circulation and extreme climatic events in the tropical Americas. *J. Atmos. Sci.,* **33,** 202–215.

——, 1985: *Climate and Circulation of the Tropics.* D. Reidel, 455 pp.

——, 1990: Prediction of northeast Brazil rainfall anomalies. *J. Climate,* **3,** 893–904.

——, and L. Heller, 1977: Dynamics of climatic hazards in Northeast Brazil. *Quart. J. Roy. Meteor. Soc.,* **103,** 77–92.

——, and P. J. Lamb, 1977: Some aspects of circulation and climate over the eastern equatorial Atlantic. *Mon. Wea. Rev.,* **105,** 1019–1023.

——, and L. Greishar, 1993: Further work on the prediction of northeast Brazil rainfall anomalies. *J. Climate,* **6,** 743–758.

Hurrell, J. W., J. J. Hack, B. A. Boville, D. L. Williamson, and J. T. Kiehl, 1998: The dynamical simulation of the NCAR Community Climate Model version 3. *J. Climate,* **11,** 1207–1236.

Kalnay, E., and Coauthors, 1996: The NCEP–NCAR 40-year Reanalysis Project. *Bull. Amer. Meteor., Soc.,* **77,** 437–471.

Kiehl, J. T., J. J. Hack, G. B. Bonan, B. P. Boville, D. L. Williamson, and P. J. Rasch, 1998: The National Center for Atmospheric Research Community Climate Model: CCM3. *J. Climate,* **11,** 1131–1149.

Kushnir, Y., and I. M. Held, 1996: Equilibrium atmospheric response to North Atlantic SST anomalies. *J. Climate,* **9,** 1208–1220.

Lamb, P. J., 1978a: Large scale tropical Atlantic surface circulation patterns associated with sub-Saharan weather anomalies. *Tellus,* **30,** 240–251.

——, 1978b: Case studies of tropical Atlantic surface circulation patterns during recent sub-Saharan weather anomalies: 1967 and 1968. *Mon. Wea. Rev,* **106,** 482–491.

Lough, J. M., 1986: Tropical Atlantic sea surface temperatures and rainfall variations in subsaharan Africa. *Mon. Wea. Rev.,* **114,** 561–570.

Mechoso, C. R., and Coauthors, 1995: The seasonal cycle over the tropical Pacific in coupled ocean–atmosphere general circulation models. *Mon. Wea. Rev.,* **123,** 2825–2838.

Mehta, V. M., 1998: Variability of the tropical ocean surface temperatures at decadal–multidecadal timescales. Part I: The Atlantic Ocean. *J. Climate,* **11,** 2351–2375.

Moura, A., and J. Shukla, 1981: On the dynamics of droughts in northeast Brazil: Observations, theory, and numerical experiments with a general circulation model. *J. Atmos. Sci.,* **38,** 2653–2675.

Palmer, T. N., and Z. Sun, 1985: A modeling and observational study of the relationship between sea surface temperature in the northwest Atlantic and the atmospheric general circulation. *Quart. J. Roy. Meteor. Soc.,* **111,** 947–975.

Peng, S., W. A. Robinson, and M. R. Hoerling, 1997: The modeled atmospheric response to midlatitude SST anomalies and its dependence on background circulation states. *J. Climate,* **10,** 971–987.

Rajagopalan, B., Y. Kushnir, and Y. M. Tourre, 1998: Observed decadal midlatitude and tropical Atlantic climate variability. *Geophys. Res. Lett.,* **25,** 3967–3970.

Rao, V. B., M. C. De Lima, and S. H. Franchito, 1993: Seasonal and interannual variations of rainfall over eastern northeast Brazil. *J. Climate,* **6,** 1754–1763.

Robertson, A. W., C. R. Mechoso, and Y.-J. Kim, 1998: The influence of Atlantic sea surface temperature anomalies on the North Atlantic Oscillation. *J. Climate,* **13,** 122–138.

Saravanan, R., 1998: Atmospheric low-frequency variability and its relationship to midlatitude SST variability: Studies using the NCAR Climate System Model. *J. Climate,* **11,** 1386–1404.

——, and P. Chang, 2000: Interaction between tropical Atlantic variability and El Niño–Southern Oscillation. *J. Climate,* **13,** 2177–2194.

Servain, J., 1991: Simple climatic indices for the tropical Atlantic Ocean and some applications. *J. Geophys. Res.,* **96,** 15 137–15 146.

Smith, T. M., R. W. Reynolds, R. E. Livezey, and D. C. Stokes, 1996: Reconstruction of historical sea surface temperatures using empirical orthogonal functions. *J. Climate,* **9,** 1403–1420.

Trenberth, K. E., G. W. Branstator, D. Karoly, A. Kumar, N.-C. Lau, and C. Ropelewski, 1998: Progress during TOGA in understanding and modeling global teleconnections associated with tropical sea surface temperatures. *J. Geophys. Res.,* **103,** 14 291–14 324.

Venzke, S., M. R. Allen, R. T. Sutton, and D. P. Rowell, 1999: The atmospheric response over the North Atlantic to decadal changes in sea surface temperature. *J. Climate,* **12,** 2562–2584.

Visbeck, M., H. Cullen, G. Krahmann, and N. Naik, 1998: An ocean model's response to North Atlantic oscillation–like wind forcing. *Geophys. Res. Lett.,* **25,** 277–280.

Xie, P., and P. A. Arkin, 1996: Analyses of global monthly precipitation using gauge observations, satellite estimates, and numerical model predictions. *J. Climate,* **9,** 840–858.

Xie, S.-P., and Y. Tanimoto, 1998: A pan-Atlantic decadal climate oscillation. *Geophys. Res. Lett.,* **25,** 2185–2188.

Zebiak, S. E., 1993: Air–sea interaction in the equatorial Atlantic region. *J. Climate,* **6,** 1567–1586.